A LiDAR-based Evaluation of Rooftop Solar Potential in DeLand, Florida

Akshay Suresh

Independent Researcher, Chennai, TN, India
Email: akshay721@gmail.com

Abstract

The state of Florida, with access to abundant sunlight, is well positioned to transition from fossil fuel dependency to solar energy. Encouraging residential solar panel installations, particularly in small cities like DeLand, is a crucial aspect of this transition. Light Detection and Ranging (LiDAR) surveys enable detailed maps of residential neighborhoods, thereby permitting homeowners to assess the feasibility of household rooftop solar, even accounting for shading from nearby structures. Here, we leverage freely available LiDAR data to evaluate the potential for solar rooftop installations on 996 households within a 1.52 km × 1.52 km area of DeLand. Our analysis reveals that approximately 76% of these households can generate sufficient electricity to meet the average annual demand of 19.2 MWh per home in DeLand. Moreover, with Florida's net metering system, surplus electricity can be sold back to the state grid for credits. Assuming a selling rate of 11 cents per kWh, our projections suggest potential yearly profits exceeding $1000 for about 53% of households in our study area. Our findings, therefore, underscore the significant potential for widespread adoption of solar panels on residential properties in DeLand, highlighting the economic and environmental benefits of such initiatives.

Keywords

Climate Change; LiDAR; Remote Sensing; Solar Forecasting

1. Introduction

Climate change from anthropogenic greenhouse gas emissions poses a significant challenge to the sustainability of the Earth's diverse

natural ecosystems. Approximately 25% of annual greenhouse gas emissions arises from fossil fuel combustion for electricity generation (Rolnick et al., 2019). Emissions reduction in the electricity sector requires both a rapid phase-out of fossil fuels as well as a swift integration of low-carbon sources, such as solar, wind, hydroelectric, and nuclear energy, into the power grid (IPCC, 2023). To enable this transition, governments worldwide are offering subsidies for investments in renewable energy, especially solar. For instance, India, through the PM Surya Ghar Muft Bijli Yojana scheme[1], offers its citizens up to ₹78,000 in subsidy for rooftop solar installation atop residential homes. Similarly, the United States of America (US) incentivizes solar panel adoption through federal tax credits[2] valued at 30% of the installation cost until 2033.

Florida, known as the "Sunshine State," ranks as the third-largest electricity consumer in the US, trailing behind Texas and California. Despite receiving between 230 to 250 days of sunlight annually, Florida falls short in generating adequate electricity to satisfy its energy needs. In January 2024, natural gas dominated the state's energy production, contributing over 75%, while solar energy lagged behind at less than 6%. Moreover, the majority of solar output comes from utility-scale facilities with 1 MW power rating or higher. On the other hand, over 50% of power consumption happens in the residential sector, where almost all homes rely on electricity for air conditioning throughout the year[3]. With the abundance of sunlight available in Florida, solar panel adoption atop residential homes appeals as a sustainable solution to meet the state's energy demands.

Tax credits for rooftop photovoltaic adoption provide strong incentives for residential homeowners to switch to solar energy. However, many homeowners remain hesitant due to the initial high costs of rooftop solar installations and concerns about shading from nearby structures (e.g., buildings and trees). High-resolution maps of residential neighborhoods are therefore necessary to enable cost-benefit analyses of solar installations on a per-house basis.

Light Detection and Ranging (LiDAR) is a remote sensing technique that uses laser light to measure distances and create detailed 3D maps of the environment. LiDAR finds application in a variety of domains, including surveying (e.g., Carter et al. 2001; Micheletto et al. 2023), autonomous vehicles (e.g., Thakker et al. 2019; Srivastav & Mandal 2023), urban planning (e.g., Muhadi et al. 2020; Uciechowska-Grakowicz et al. 2023), forestry (e.g., Dassot et al. 2011; Alvites et al. 2022), and environmental monitor-

[1] https://pmsuryaghar.gov.in
[2] https://www.energy.gov/eere/solar/homeowners-guide-federal-tax-credit-solar-photovoltaics
[3] Florida energy usage statistics: https://www.eia.gov/state/analysis.php?sid=FL.

ing (e.g., Haugerud et al. 2003; Wang et al. 2023). In this study, we leveraged freely available LiDAR data to conduct a house-by-house assessment of the potential for rooftop solar installations in a 1.52 km × 1.52 km residential neighborhood of DeLand, Florida.

We detail our study region and sources of raw data in Section 2. Section 3 describes our data processing methodology to compute the expected annual solar energy output on a per-house basis. In Section 4, we present the results from our data analysis and share insights gleaned from our study. Finally, we summarize and conclude our investigation in Section 5.

2. Study Region and Data Sources

DeLand is a small residential city in central Florida with an estimated population[4] of 41,263 in 2023. Located approximately 55 km north of Orlando and about 37 km west of Daytona Beach, DeLand offers its residents a rural feel with close access to sprawling business districts. Family establishments comprise over 60% of households in DeLand, with most of them being owner-occupied[5]. On average, residents in DeLand consume about 19.2 MWh of energy per year, and pay approximately $3,612 in annual electricity bills[6]. This expense is roughly 66% higher than the US-averaged annual electricity bill of $2,179 per household. With the immense scope for solar energy in Florida, DeLand's residential landscape dominated by owner-occupied family homes presents a viable setting for a pilot study to assess house-wise rooftop solar potential.

The US 3D Elevation Program (3DEP: Sugarbaker et al. 2014), managed by the US Geological Survey (USGS), is an initiative to establish a comprehensive national baseline of consistent, high-resolution topographic elevation data. Launched in 2016, 3DEP data products are available free of charge to the public, including LiDAR point cloud data and digital elevation models (DEMs). For this study, we downloaded LiDAR point cloud data[7] gathered in 2019 for a 1.52 km × 1.52 km neighborhood of DeLand, Florida. Our LiDAR data come georeferenced in the NAD 1983 UTM Zone 17N coordinate frame with a point spacing of ≈ 19.2 cm. Figure 1 shows satellite imagery of the area spanned by our LiDAR data, revealing a residential setting with plenty of tree cover.

Microsoft has publicly released a dataset of 129,591,852 US building footprints[8] generated by applying computer vision models on

[4] https://www.deland.org/206/DeLand-Demographics
[5] https://www.point2homes.com/US/Neighborhood/FL/DeLand-Demographics.html
[6] https://www.energysage.com/local-data/electricity-cost/fl/volusia-county/deland
[7] LiDAR data download link: https://rockyweb.usgs.gov/vdelivery/Datasets/Staged/Elevation/LPC/Projects/FL_Peninsular_2018_D18/FL_Peninsular_Volusia_2018/LAZ/USGS_LPC_FL_Peninsular_2018_D18_LID2019_247579_E.laz
[8] https://github.com/Microsoft/USBuildingFootprints

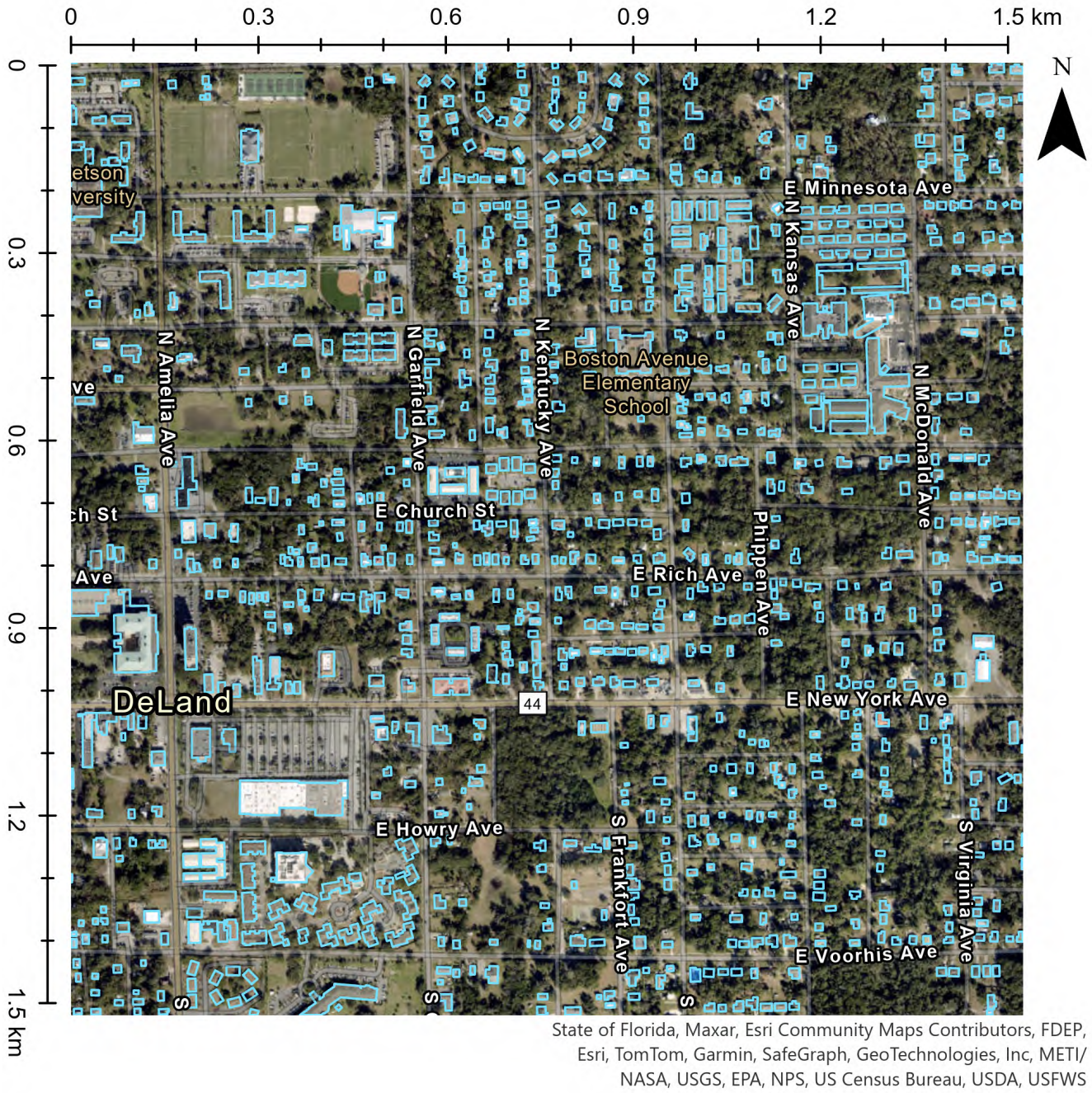

Figure 1: Study region spanning a 1.52 km × 1.52 km residential neighborhood of DeLand, Florida. Light blue outlines demarcate building footprints identified by Microsoft using computer vision models applied to Bing satellite imagery. Figure prepared using ArcGIS Pro 3.0.

Bing satellite imagery from 2012–2020. The performance of such models can be summarized using three metrics, namely the recall, the false positive rate, and the Intersection-over-Union (IoU). The recall, also called the true positive rate, measures the proportion of buildings that have been correctly detected. Meanwhile, the false positive rate quantifies the fraction of background

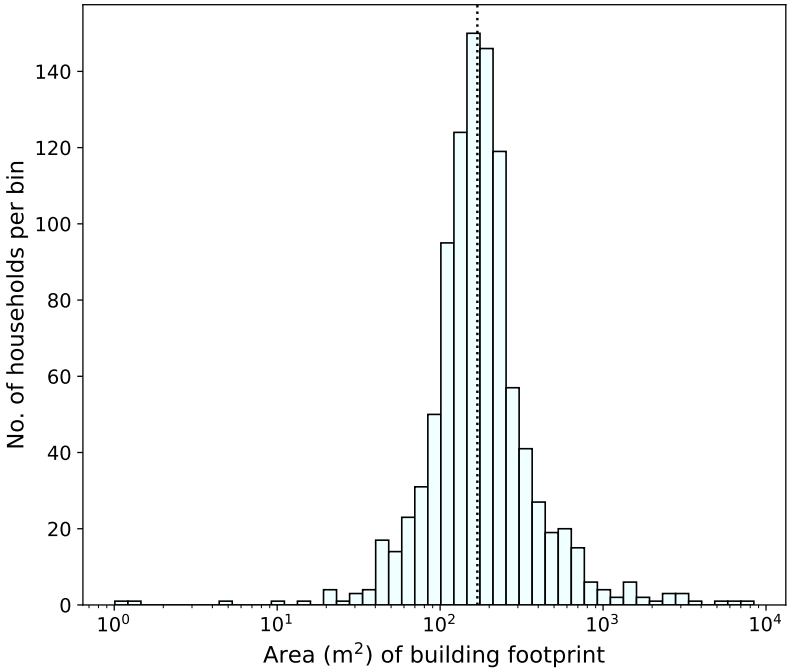

Figure 2: Histogram of footprint areas of the 996 buildings detected by Microsoft in our study region. The vertical dotted black line labels the median building footprint area of ≈ 169 m^2.

image pixels that have been incorrectly classified as being part of a building. Finally, the IoU captures the fractional spatial overlap between the detected building polygons and their corresponding ground truth extents. Microsoft, for their building footprint detection task, reported good model performance with a recall of 92%, a false positive rate of $< 1\%$, and an IoU of 86%.

For this study, we downloaded the Microsoft-generated shapefile of building outlines for the state of Florida and subsequently clipped the shapefile to the spatial extent of our LiDAR point cloud data. This clipping operation was performed using the `Clip (Analysis)` tool of ArcGIS Pro 3.0 (Environmental Systems Research Institute, Inc., 2022). Further, Microsoft specifies building outlines in the WGS 1984 coordinate reference frame. We used the `Project (Data Management)` routine of ArcGIS Pro 3.0 to transform these coordinates to the NAD 1983 UTM Zone 17N frame of our LiDAR data. Finally, we computed the footprint area enclosed by every building in our clipped shapefile.

Figure 2 presents a histogram of footprint areas of the 996 buildings detected by Microsoft in our study region. Our study region evidently encompasses four orders of magnitude in building footprint size, with a median footprint area of ≈ 169 m^2.

Table 1: LiDAR class codes and data coverage

Class code	Surface category	No. of data points	Percentage data coverage (%)
1	Unclassified	36,349,581	57.7 %
2	Ground	22,270,867	35.4 %
6	Buildings	4,194,020	6.7 %
7	Low point (noise)	150,915	0.2 %
18	High noise	2	$\approx 3 \times 10^{-6}$ %
-	All	62,965,385	100 %

Table 2: Statistics of laser returns in our LiDAR point cloud data

Return category	Point count	Percentage data coverage (%)
First	52,075,709	82.7 %
Second	9,256,230	14.7 %
Third	1,345,366	2.1 %
Fourth	255,278	0.4 %
Fifth	30,592	$\approx 5 \times 10^{-2}$ %
Sixth	2,138	$\approx 3 \times 10^{-3}$ %
Seventh	71	$\approx 10^{-4}$ %
Eighth	1	$\approx 2 \times 10^{-6}$ %
Last	51,846,015	82.3 %
Single	42,598,031	67.7 %
First of many	9,477,678	15.1 %
Last of many	9,247,984	14.7 %
All	62,965,385	100 %

3. Data Analysis Methodology

3.1. Generation of Topographic Maps from LiDAR Data

LiDAR data points are assigned numerical class codes to classify between different types of objects or surfaces encountered. In addition, each individual laser pulse may yield one or more returns based on the incident surface texture. Tables 1 and 2 provide statistics of various class codes and laser return categories seen in our LiDAR point cloud data.

A DEM measures the elevation of the bare Earth surface relative to mean sea level. DEMs exclude surface objects such as buildings, vegetation, or infrastructure, from their representations. On the other hand, a digital surface model (DSM) captures the Earth's surface as seen from overhead imagery.

Grouping all returns from ground points (class code 2), we built a DEM of our study region using the `LAS Dataset to Raster (Conversion)` tool of ArcGIS Pro 3.0. Similarly, we constructed a DSM using LiDAR data points with the return categories "First" and "First of many." Figure 3 shows our DEM (left) and DSM (right), both of which share a common pixel resolution of ≈ 76 cm. We compare our DEM against that publicly released

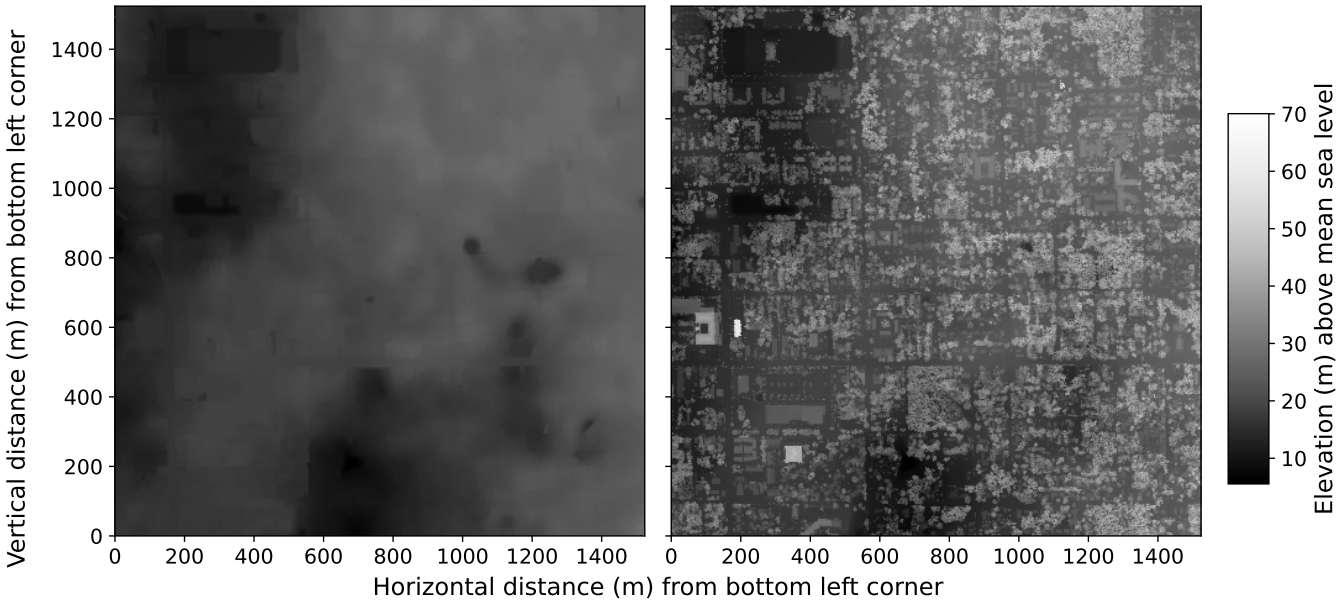

Figure 3: DEM (left) and DSM (right) generated from LiDAR point cloud data of our study region.

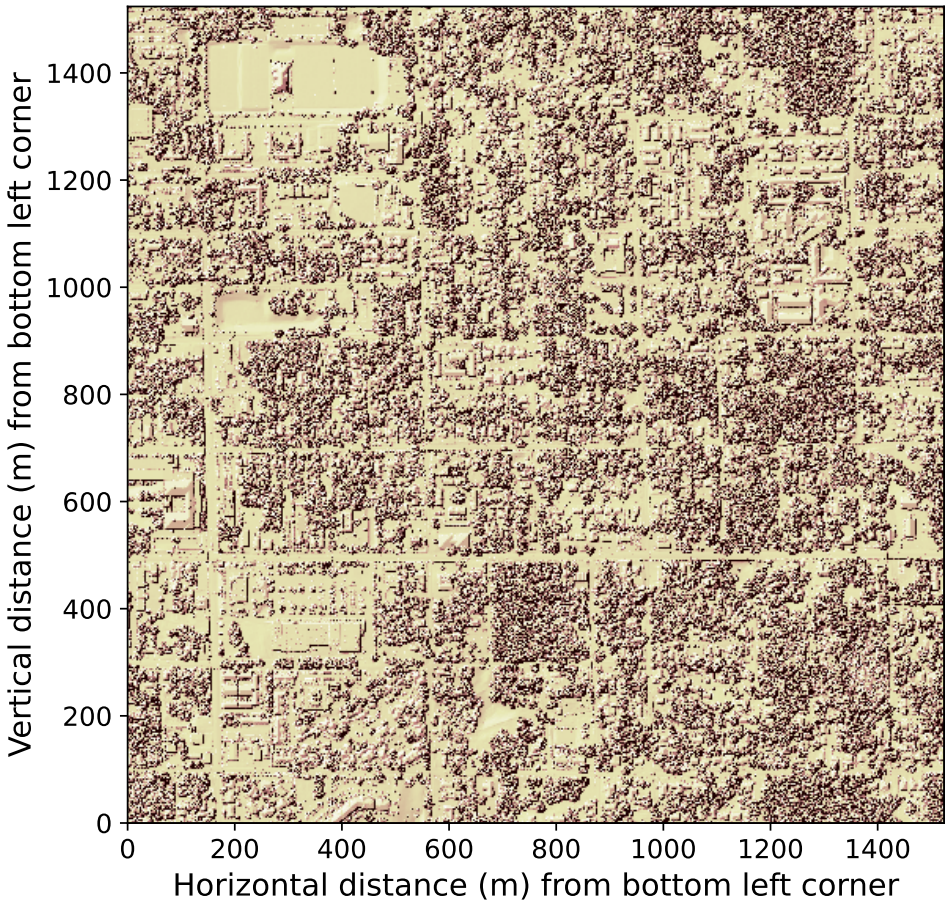

Figure 4: DSM with hillshade raster function applied to reveal structures, including sloped roofs, pavements, and trees. A solar altitude of 45° and a solar azimuth of 315° was assumed for deriving the hillshade effect with ArcGIS Pro 3.0.

by USGS[9] and obtain a 99.9% match at the pixel level. In Figure 4, we apply a hillshade raster function to reveal structures in our DSM, including sloped rooftops, pavements, and trees. This hillshade effect was computed in ArcGIS Pro 3.0 assuming a solar altitude of 45° and a solar azimuth of 315°.

3.2. Calculation of Pixel-level Solar Insolation

The top of the Earth's atmosphere receives an instantaneous solar radiation flux of $\approx$ 1361 W/m^2. As this incoming light encounters dust, air molecules, and clouds in the Earth's atmosphere, it gets absorbed and scattered, leading to a reduction in its intensity. In general, the Earth's atmosphere transmits between 30–70 % of the incoming solar energy to the surface (Srivastava et al., 2021). However, not all the transmitted power gets captured by solar panels.

During daytime, sunlight can reach a solar panel in three different ways. First, rays of sunlight may directly arrive at a panel unobstructed. Second, a panel may receive diffuse sunlight that has been scattered by clouds and dust in the Earth's atmosphere. Third, a panel may receive radiation reflected from the ground. Among these three means of energy reception, the last mode is generally negligible for sky-directed monofacial rooftop panels. Hence, we consider only the first two energy reception pathways in our assessment of rooftop solar potential.

Two critical parameters governing solar panel output are the panel tilt, $\theta_{\mathrm{PV}} \in [0°, 90°]$, and orientation, $\phi_{\mathrm{PV}} \in [0°, 360°)$. The panel tilt is the angle between the solar panel surface and the ground plane. Meanwhile, the panel orientation is an azimuthal angle in the ground plane measured counterclockwise (north to east) relative to true north at $\phi_{\mathrm{PV}} = 0°$. The orientation, therefore, labels the direction in which the solar panel faces.

In our study, we assume that all solar panels are fixed installations with tilts and orientations following the that of their underlying rooftops. A general rule of thumb for maximizing power generation with such space-fixed solar panels is to install panels facing south in the northern hemisphere and north in the southern hemisphere. However, at sufficiently low latitudes, alternate panel orientations may also deliver substantial power for household electricity consumption.

The solar insolation of a surface in time T is defined as the cumulative solar energy received per unit area normal to the surface. Measured in kWh/m^2, the pixel-level solar insolation can be calculated for homes in

[9]USGS-supplied DEM: https://rockyweb.usgs.gov/vdelivery/Datasets/Staged/Elevation/OPR/Projects/FL_Peninsular_2018_D18/FL_Peninsular_Volusia_2018/TIFF/USGS_OPR_FL_Peninsular_2018_D18_DEM247579.tif

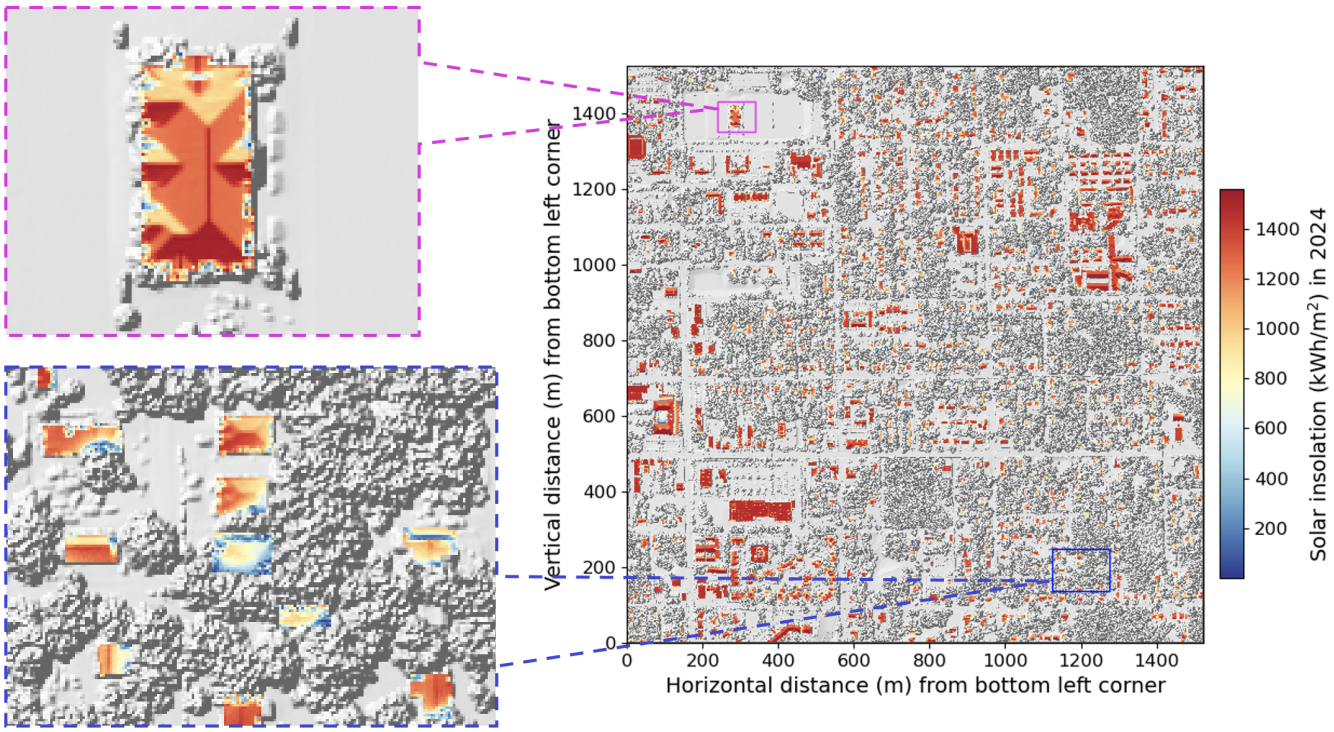

Figure 5: A map of pixel-level solar insolation estimates. Left insets show zoomed-in views of the right panel for two specific localities. The top left inset demonstrates solar insolation values for a single home surrounded by trees. Evidently, solar insolation values are lower at roof bottoms due to shading from adjacent trees. The bottom left inset shows a collection of homes, where shade from tree cover significantly diminishes solar insolation near the edges of various building rooftops.

our study region using the `Area Solar Radiation (Spatial Analyst)` method of ArcGIS Pro 3.0. This functionality evaluates the net solar insolation per pixel of a DSM by considering the surface slope, the surface aspect, and the sky positions of the Sun at multiple times throughout a day and on multiple days throughout a year.

Section 4.1 presents our pixel-level solar insolation raster prepared with the `Area Solar Radiation (Spatial Analyst)` routine. For our analysis, we assumed $T = 1$ year (2024) and evaluated sky positions of the Sun once every 30 minutes for one day per two weeks of the year. Further, we applied the standard overcast sky model in ArcGIS Pro 3.0, with a presumed atmospheric transmissivity of 50% and a diffuse proportion of 30%. The diffuse proportion captures the fraction of global normal radiation flux that is in the diffuse or scattered component of the radiation incident on a solar panel.

3.3. Computation of Household Solar Energy Production

With access to our shapefile of building footprints and pixel-level solar insolation values, we derived estimates of the household solar energy production, E, as follows.

$$E = \epsilon \Upsilon \, (\text{Footprint Area}) \, (\text{Footprint-averaged solar insolation}) \, . \qquad (1)$$

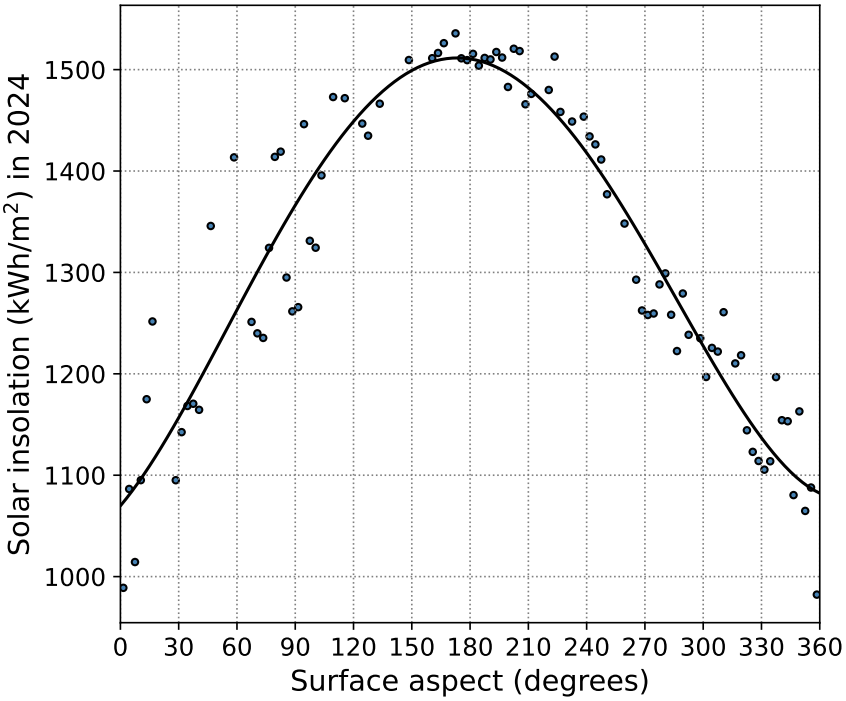

Figure 6: Variation of solar insolation with rooftop orientation (surface aspect) for the household shown in the top left panel of Figure 5. Aspect values of 0°, 90°, 180°, and 270° represent north, east, south, and west respectively. The solid black curve is a quartic polynomial fitted to the dark blue scatter points.

Here, ϵ and Υ are the efficiency and performance ratio of the solar panel respectively. The solar panel efficiency measures the fraction of incoming solar energy converted into electricity. Meanwhile, the performance ratio quantifies the proportion of generated electrical energy that is preserved through the panel installation. For our study, we assume $\epsilon = 22\%$[10] and $\Upsilon = 80\%$[11], which are representative values for commercially manufactured solar panels in 2024.

4. Results and Discussion

4.1. Trends in Pixel-level Solar Insolation

Figure 5 displays solar insolation estimates for buildings in our study area, revealing shading effects from nearby trees. South-facing rooftops receive the highest insolation, especially evident from pixels with $\gtrsim 1000$ kWh/m^2 insolation. Figure 6 highlights this trend, using the building in the top left inset of Figure 5 as an example.

4.2. Evaluation of House-wise Rooftop Solar Potential

Figure 7 illustrates a web map[12] screenshot showcasing solar energy production estimates for homes in our study region during the year 2024. We deduce that roughly 76% of homes can generate sufficient solar energy to

[10] https://www.energysage.com/solar/what-are-the-most-efficient-solar-panels-on-the-market/
[11] https://www.energy.gov/sites/default/files/2022-02/understanding-solar-photo-voltaic-system-performance.pdf
[12] **Web map URL:** https://arcg.is/19eKXP0

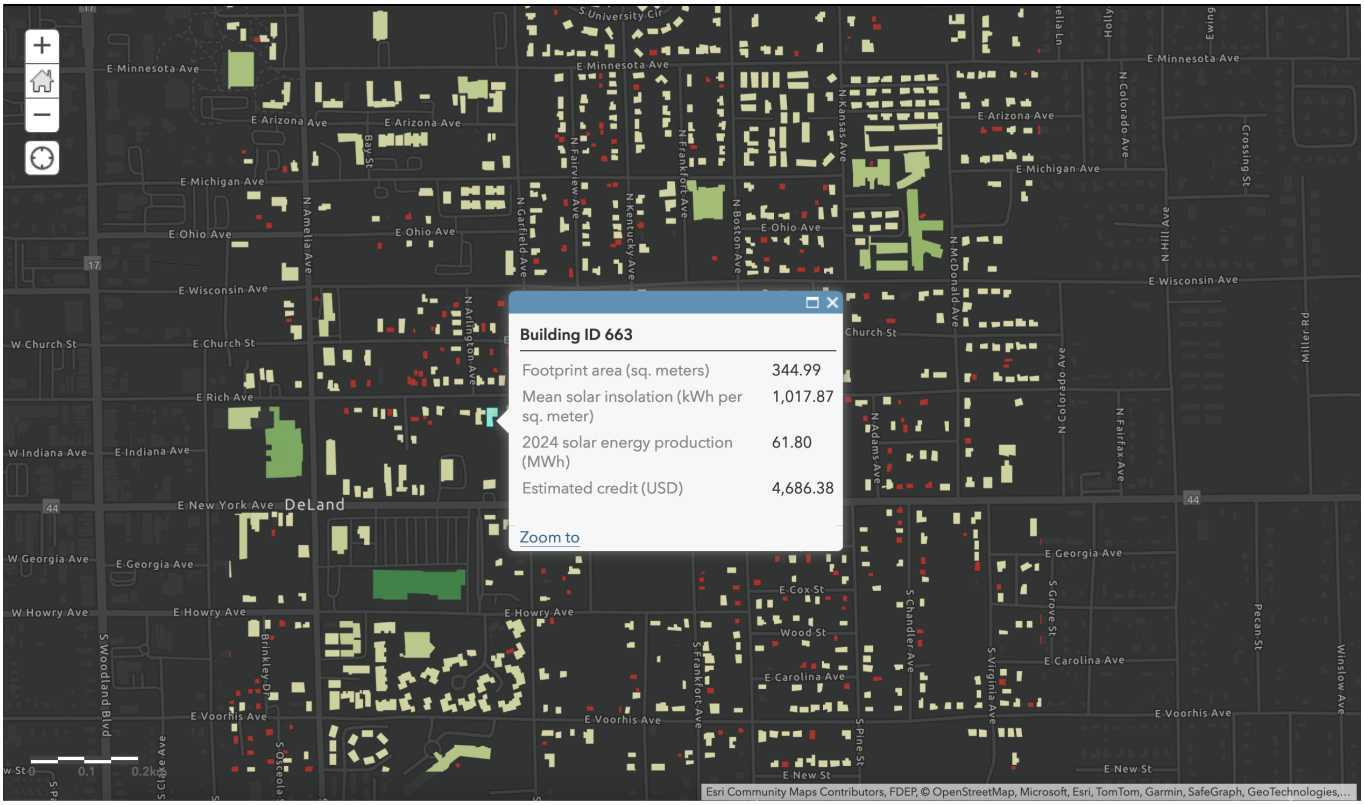

Figure 7: Screenshot of a web map illustrating household-level solar energy production estimates (E) for 2024. Households shaded in green have E values exceeding the DeLand average of 19.2 MWh per home. Darker shades of green correspond to higher values of E. Buildings labeled in red have $E < 19.2$ MWh. In this study, we presumed a constant annual energy demand of 19.2 MWh for all buildings irrespective of home area. Credits from sale of surplus generated solar power to the state grid are computed assuming a selling rate of 11 cents per kWh. Web map hosted on ArcGIS Online.

meet the average annual demand of 19.2 MWh per household in DeLand. Additionally, Florida's net metering system allows households to earn credits for supplying surplus generated electricity to the state power grid. Based on a selling rate of 11 cents per kWh (2017 data[13]), about 53% of households stand to receive over $1000 in potential credits. Here, we assume that households of all sizes share a common annual energy demand of 19.2 MWh.

Figure 8 shows the marginal distribution of household solar energy production as a function of building footprint area. Fitting a power-law model, we infer that an annual energy requirement of 19.2 MWh warrants a minimum home area of ≈ 108 m^2.

4.3. Areas for Improvement

We encourage exploring potential enhancements in our presented conclusions, particularly by relaxing several simplifying assumptions made throughout our study. For example, our calculation of pixel-level solar insolation can benefit from incorporation of historical climate data and detailed cloud cover assessments using satellite imagery and numerical weather prediction models. Additionally, when evaluating credits earned by households

[13] https://www.energysage.com/local-data/net-metering/fpl/

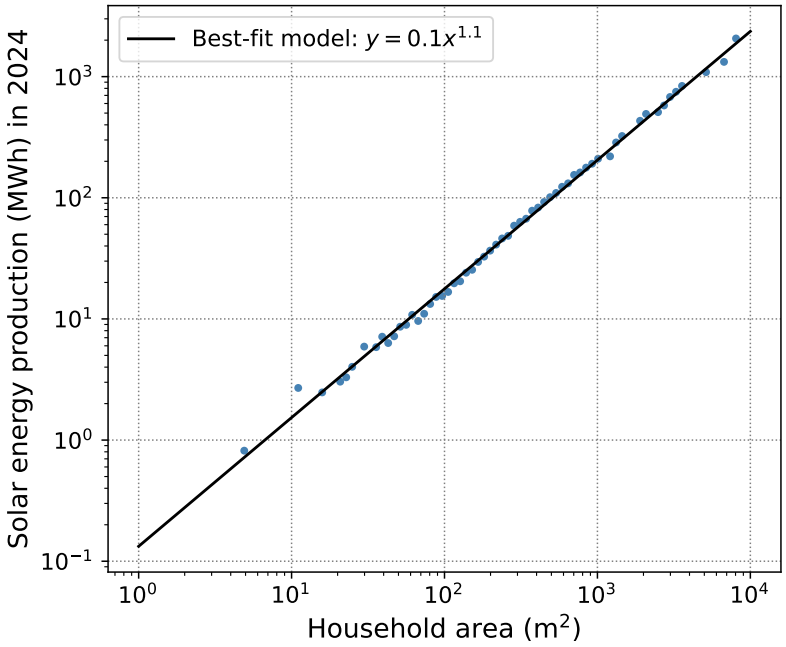

Figure 8: Distribution of household solar energy production as a function of home area after marginalization over building-averaged solar insolation. Generation of the DeLand average annual energy demand of 19.2 MWh per household requires a minimum home area of ≈ 108 m^2.

selling excess solar energy to the state grid, considering variable energy requirements based on home sizes, occupancy, and appliance usage patterns could offer a more accurate representation of reality. Ultimately, addressing limitations on solar energy production imposed by regulations governing the installation capacities of solar cells on residential properties of different sizes is crucial for building a comprehensive assessment of rooftop solar potential.

5. Summary and Conclusion

Solar energy offers a viable alternative to fossil fuel combustion in the quest to minimize global greenhouse gas emissions from the power generation industry. Florida, with access to an abundance of sunlight, is favorably positioned to lead this transition. A key element to embracing solar energy is providing residential homeowners in small cities with accurate assessments of the profitability of household rooftop solar installations, accounting for shading from nearby structures. High-resolution maps of residential neighborhoods gathered with remote sensing techniques such as LiDAR are therefore essential to conduct plausibility studies for rooftop solar potential.

Here, we leveraged freely available LiDAR data to evaluate rooftop solar potential for 996 households in a 1.52 km $\times$ 1.52 km study region. Our study area is based in DeLand, a small residential city in Central Florida with a mean yearly household energy consumption of 19.2 MWh. In the absence of granular knowledge of the annual elec-

tricity consumption for each building, we assume every household in our study to uniformly require the mean energy demand of 19.2 MWh per year.

Our investigation builds upon two data sources — LiDAR data from the 3DEP program, and a shapefile of US building footprints produced by Microsoft using artificial intelligence. Using these data inputs, we constructed two output products — a raster map of pixel-level solar insolation per building for the year 2024 and a web map of annual household solar energy production estimates. We estimate that 757 households ($\approx$ 76% of homes) in our study region receive adequate solar exposure to meet the annual average demand of 19.2 MWh per home. Further, production of at least 19.2 MWh of solar energy necessitates a minimum home area of ≈ 108 m^2.

Florida has an active net metering system that pays residents for selling excess generated solar energy to the state power grid. Assuming a selling rate of 11 cents per kWh, 529 buildings ($\approx$ 53% of homes) in our study area stand to generate annual profits exceeding $1000, thereby, highlighting the economic potential for widespread rooftop solar adoption in DeLand.

Acknowledgement

AS thanks Prita Nair (Shiv Nadar University, Chennai) for thought-provoking discussions that informed the direction of this work. AS acknowledges Malin Hansepi (GIS Vision India) for supplying valuable technical guidance with ArcGIS Pro 3.0.

References

Alvites, C., Marchetti, M., Lasserre, B., & Santopuoli, G. 2022, Remote Sensing, 14, 4466, doi: 10.3390/rs14184466

Carter, W., Shrestha, R., Tuell, G., Bloomquist, D., & Sartori, M. 2001, EOS Transactions, 82, 549, doi: 10.1029/01EO00321

Dassot, M., Constant, T., & Fournier, M. 2011, Annals of Forest Science, 68, 959, doi: 10.1007/s13595-011-0102-2

Environmental Systems Research Institute, Inc. 2022, ArcGIS Pro 3.0. https://www.esri.com/en-us/arcgis/products/arcgis-pro/overview

Haugerud, R. A., Harding, D. J., Johnson, S. Y., et al. 2003, GSA Today, 13, 4, doi: 10.1130/1052-5173(2003)13⟨0004:HLTOTP⟩2.0.CO;2

IPCC. 2023, Climate Change 2023: Synthesis Report. Contribution of Working Groups I, II and III to the Sixth Assessment Report of the Intergovernmental Panel on Climate Change, ed. H. Lee & J. Romero (Geneva, Switzerland: IPCC), doi: 10.59327/IPCC/AR6-9789291691647

Micheletto, M. J., Chesñevar, C. I., & Santos, R. 2023, Sensors, 23, 7212, doi: 10.3390/s23167212

Muhadi, N. A., Abdullah, A. F., Bejo, S. K., Mahadi, M. R., & Mijic, A. 2020, Remote Sensing, 12, 2308, doi: 10.3390/rs12142308

Rolnick, D., Donti, P. L., Kaack, L. H., et al. 2019, arXiv e-prints, arXiv:1906.05433, doi: 10.48550/arXiv.1906.05433

Srivastav, A., & Mandal, S. 2023, IEEE Access, 11, 97147, doi: 10.1109/ACCESS.2023.3312382

Srivastava, A., Rodriguez, J. F., Saco, P. M., Kumari, N., & Yetemen, O. 2021, Remote Sensing, 13, 1716, doi: 10.3390/rs13091716

Sugarbaker, L. J., Constance, E. W., Heidemann, H. K., et al. 2014, US Geological Survey Circular 1399, 35, doi: 10.3133/cir1399

Thakker, T., Pulikkaseril, C., Lam, S., & Shen, D. 2019, in Society of Photo-Optical Instrumentation Engineers (SPIE) Conference Series, Vol. 11200, Society of Photo-Optical Instrumentation Engineers (SPIE) Conference Series, ed. A. Mitchell & H. Rubinsztein-Dunlop, 112001N, doi: 10.1117/12.2552778

Uciechowska-Grakowicz, A., Herrera-Granados, O., Biernat, S., & Bac-Bronowicz, J. 2023, Remote Sensing, 15, 5776, doi: 10.3390/rs15245776

Wang, J., Wang, L., Feng, S., et al. 2023, Remote Sensing, 15, 253, doi: 10.3390/rs15010253